Analysis of the flow produced by a low–Reynolds rotor optimized for low noise applications. Part II: Acoustics

R. Serré*†, Nicolas Gourdain†, Thierry Jardin†, Gregory Delattre‡ and J.–M. Moschetta†
† Department of Aerodynamics, Energetics and Propulsion (DAEP), ISAE–Supaero, Toulouse, France
‡ Department of Applied Aerodynamics (DAAP), ONERA, Toulouse, France

Abstract

The demand in Micro–Air Vehicles (MAV) is increasing as well as their potential missions. Whether for discretion in military operations or noise pollution in civilian use, noise reduction of MAV is a goal to achieve. This contribution briefly describes a low–cost, numerical methodology to achieve noise reduction by optimization of MAV rotor blade geometry. It is suited for engineering purposes and dedicated to low–Reynolds number rotors. That methodology is applied to reduce noise from a MAV developped at ISAE–Supaero and a 8 dB(A) reduction on the acoustic power is found experimentally. Noise due to turbulence ingestion is found to be the dominant source of noise in MAV rotors. The innovative rotor blade geometry allowing this noise reduction is then analyzed in detail using high–fidelity numerical approaches such as Unsteady Reynolds Averaged Navier–Stokes (URANS) simulation and Large Eddy Simulation using Lattice Boltzmann Method (LES–LBM). That strategy gives insight on the flow features around the optimized rotor to allow higher noise reduction through passive control devices such as leading edge tubercles.

Keywords: Aeroacoustics, optimization, low–Reynolds number, Micro–Air Vehicle

1 INTRODUCTION

Designing a silent rotor goes through an aeroacoustic optimization, which implies understanding the aerodynamic phenomena responsible for noise generation. Predicting the noise generated aerodynamically is relatively straightforward once detailed aerodynamics involved in the propulsion system are available through the use of direct noise computation or hybrid prediction. Aeroacoustic optimization in that framework is possible[1,2] but demanding in terms of computational cost hence not realistic in an industrial context. To this aim, lower–fidelity tools are needed. The numerical tool discussed in the present paper is suited for engineering purposes. It contains an aerodynamic model, acoustic models for tonal and broadband noise and optimization algorithms. A similar strategy has been followed by Wisniewsky *et al.*[3] and Zawodny *et al.*[4] with models based on empirical data at relatively high Reynolds numbers and for symetrical profile. The present study proposes a more general methodology. The optimization consists in a systematic scanning of the parameters space defined by chord and twist laws as a function of the blade radius and rotor rotation speed with constant thrust as objective. The blade chord and twist laws are parameterized by Bézier curves considering control points in 4 sections along the blade span giving 8 variables. However, in order to ensure that lift at blade tip vanishes, which is required to minimize induced velocity, the twist at the fourth control point is set to zero eventually giving 7 variables. In the combination method, each variable can take 4 values giving 4^7 individual evaluations. A multi–objective selection is applied to express the pareto front according to lower power consumption and lower overall sound pressure level. The numerical tool allows airfoil section optimization although this paper focuses on investigating one optimized geometry previously obtained. The effect of the airfoil section optimization has been addressed in a companion paper[5] and will not be discussed hereafter. It is carried out in a second step through another optimization process. This second optimization is carried out with the NSGA–II evolutionary algorithm through CST airfoil parametrization to maximize is the lift-to-drag ratio.

2 AERODYNAMIC MODELING

For each set of parameters, the blade loading is obtained using Blade Element and Momentium Theory (BEMT) as described by Winarto[6]. Distributions of lift and drag and global thrust and torque are retrieved from local lift and drag coefficients of the blade element airfoil sections. Knowledge of the aerodynamic polar of the considered airfoil section is essential. Three strategies may be employed to this end: experimental[7], high–fidelity simulation[8] or low–fidelity modeling[9]. The last one is used in the present study for efficiency reasons. Lift and drag coefficients are extracted from Xfoil open–source software by Drela[9], as well as boundary layer data. That software is based on potential theory with viscosity models. It was shown in a previous paper[5] that Xfoil provides results in agreement with

*Email address: ronan.serre@isae.fr

experiments. For that reason, it is used herein to provide input data to the optimization tool. The aerodynamic model based on BEMT is fast and reliable but yields a steady loading on the blades and that reduces *a priori* the ability to predict noise radiation, for acoustic is intrinsically unsteady. However, because of the relative motion between the spinning blades and a static observer, acoustic radiation can still be retrieved from a steady loading but only the main tonal part from the periodic excitation. As stated by Sinibaldi and Marino[10], the acoustic spectrum radiated by rotors exhibits also a broadband part. Low–fidelity broadband models are added in the optimization process to enrich the acoustic prediction.

3 ACOUSTIC MODELING

The acoustic modeling is realized in two steps: *i)* an integral method based on the Ffowcs Williams and Hawkings[11] (FWH) equation gives the tonal noise radiated by the rotor from the steady loading yielded by the BEMT and *ii)* analytical models estimate the broadband part of the acoustic spectrum based on the work of Roger and Moreau[12]. The FWH equation is implemented in the time domain as expressed by Casalino[13] in the form known as Formulation 1A[14] and applied on the blade surface. The quadrupole term is removed from the FWH equation and since the integration surfaces correspond to the blades, no quadrupole source is taken into account. This is physically consistent with the low Mach number context of the MAV rotors[10]. As a consequence, the FWH reduces to thickness and loading noise computation obtained from the two surface integrals. The main input parameters are the incoming flow velocity at the blade element influencing the thickness noise and the force distributions acting on the loading noise. In that steady loading framework, the latter is found to be relatively small without significantly contributing to the overall noise while the former is found to be dominant independently of the observer's location. This discussion is addressed at the end of the paper. In addition, two sources of broadband noise are considered: the scattering of boundary layer waves by the trailing edge and the ingestion of turbulence at the leading edge[12]. The main input for the trailing edge noise model is a wall pressure spectrum model as proposed by Kim and George[15]. The driving parameters for the interaction noise model is a the turbulence length scale and the turbulence intensity. LBM simulation discussed in the present paper has provided these informations and helped calibrate a scaling parameter in the optimization tool[16]. Power spectral density are then retrieved from the models with a correlation function modified by a Doppler shift imposed by the relative motion between the source and the observer. Note that during the optimization process, only one observer location is considered, located $45\,°$ above the rotor plane, 1 m away from the center of rotation. This location has been chosen as a compromise according to the directivity yielded by the optimization tool[5]. Formulation 1A of the FWH equation gives a singular value on the axis of rotation while the broadband noise models have a singularity in the rotor plane.

4 EXPERIMENTAL PROCEDURE

The optimization tool is used at ISAE–Supaero to determine a low noise MAV blade geometry. Chord and twist distribution laws were derived from a range of possibilities in the spanwise chord–twist space for several numbers of blades per rotor at constant thrust of 2.85 N required for hovering flight, allowing for rotational speed to adjust. The airfoil section is a Gottingen 265 for it is a thin, cambered airfoil suitable for low Reynolds number flow. The conventional rotor compared to the optimized configurations is a two–blade commercial rotor with APC7x5 blades, mounted on the ISAE–Supaero MAV. Since the airfoil section of APC7x5 blades wass unknown to the authors, the conventional rotor and the best optimized one are compared experimentally. The optimized rotors are manufactured using SLA technology on a $3D$ printer with a 50 μm vertical resolution.

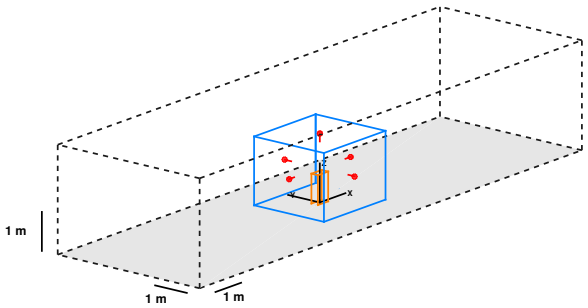

Figure 1: Schematic view of the experimental set–up following the ISO $3746:1995$ standard. The source (orange) is surrounded by the measurement surface (blue) on which the microphones are positionned (red).

The measurements take place in a rectangular room, acoustically non–treated of dimensions $(l_1 \times l_2 \times l_3) = (14.9 \times 4.5 \times 1.8)$ m^3. The aerodynamic forces are retrieved from a five components balance. The sound power level is computed according to ISO $3746:1995$ standard with five measurement points 1 m around the rotor as illustrated in figure 1, on a Brüel & Kjær $1/2''$ free–field microphone and a Nexus frequency analyzer with a frequency resolution of 3.125 Hz. The distance between the source and the microphones approximately represents 5 rotor diameters. Four of the microphones are on a meridian line parallel to the ground and centered on the axis of rotation and a fifth microphone is located in the plane of rotation. The experimental procedure is currently being set in an anechoic chamber recently delivered to ISAE–Supaero. The maximum noise reduction for the optimized geometries is achieved by the three–blade configuration according to measurements[16]. Its chord and twist distribution laws

are plotted in figure 2 with those of the conventional rotor. The radial position is normalized by maximum radius of the blade $R = 0.0875$ m. The optimized chord is larger while the twist laws are approximately the same, except at 75% of blade span where the optimized twist increases again before vanishing at the tip.

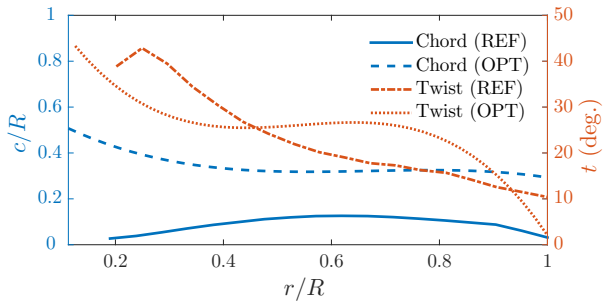

Figure 2: Chord and twist distribution laws for the conventional rotor ("REF") and the optimized rotor ("OPT"). Normalized by tip radius $R = 0.0875$ m.

5 INVESTIGATION OF THE OPTIMIZED ROTOR

The optimized rotor is investigated with high–fidelity numerical simulation as discussed in the first part of the present contribution. For acoustic purposes, only the LBM simulation is hereby discussed. Analyzing the characteristics of the optimized geometry with high–fidelity numerical simulations helps validate the aerodynamic model in the optimization tool and the acoustic broadband models and gives informations on the noise sources ranking in MAV rotors. Analyzing the LBM simulation also provides informations on the flow features around the optimized rotor and helps identify specific characteristics such as leading edge separation as can be seen on figure 3. Such a phenomenon occurs around 75% of the blade radius, where the twist angle increases again (figure 2) suggesting that having an inflection point on the twist distribution law should be avoided. The resulting flow then merges with the tip vortex and impinges the following blade. It creates an interaction noise that is believed by the authors to be the most dominant noise source in this configuration[16]. This supports the idea that passive control devices on the leading edge may reduce interaction noise and significantly decrease the acoustic power radiated.

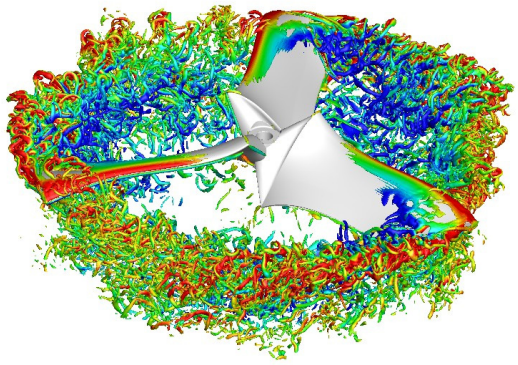

Figure 3: Iso–surface of Q–criterion colored by longitudinal velocity for the optimized rotor at $5,000$ rpm. LBM simulation.

An aeroacoustic solver is developped to predict the noise from the LBM simulation. It solves the FWH equation in the frequency domain[17] on a cartesian, porous surface surrounding the optimized rotor. The porous surface is centered on the rotor and is two rotor diameters long in the directions parallel to the rotor plane and one rotor diameter long in the direction parallel to the axis of rotation. Aerodynamic data are extracted for three rotor revolutions with a high frequency resolution that is approximately a third of the blade passing frequency or 30 Hz. The purpose is first to assess the ability of LBM simulation to provide valuable information for wave propagation methods[18]. It is believed that LBM simulation is a natural candidate for providing aerodynamic input to aeroacoustic analogies if care is taken to ensure that eddies do not cross the control surfaces. It is brought to the reader's attention that a filtering procedure has been addressed recently in reference[19] to suppress spurious signal from porous FWH solver but does not appear mature. A weighting coefficient is applied on the multipole definitions as suggested by Lockard[20]. That FWH–LBM tool is used for comparison with measurements and prediction from the optimization tool. The same procedure will be applied with U–RANS simulations discussed in the first part of the present paper when the appropriate data are available. Acoustic power L_{wA} computed according to ISO $3746 : 1995$ standard is plotted on figure 4 for a range of rotational speeds from measurements (labelled "Exp" for experimental), LBM simulation (labelled "LBM") and optimization tool with noise models activated separately. It is referred as "TN" when only tonal noise is considered, "TE" when the trailing edge broadband noise model is activated in addition to the tonal noise and "TI" when interaction broadband noise model is activated. The optimization tool and the FWH–LBM yield higher acoustic power than the measurements. On the one hand, the overestimation from the optimization tool might be a consequence of the approximation discussed in reference[16] of the two driving parameters: the turbulence length scale and the turbulence

intensity. On the other hand, the overestimation from the FWH–LBM tool might be a consequence of the large frequency resolution currently available.

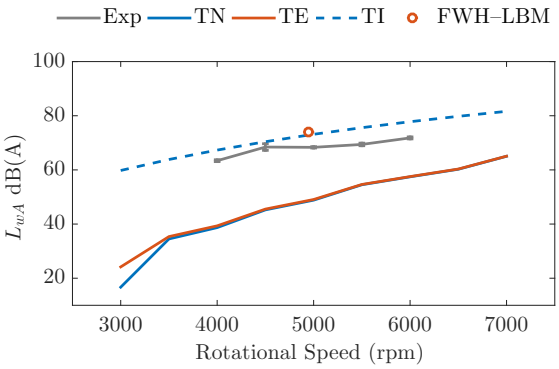

Figure 4: Acoustic power with rotational speed from measurements with standard deviation and numerical predictions.

This slight overestimation notwithstanding, the interaction noise model is relevant and allow a prediction of the optimization tool right between the measurements and the FWH–LBM tool prediction. The prediction from the trailing edge noise model or from the tonal noise model are both underneath the measurements. This observation indicates that interaction noise is the dominant source of noise in this context and that the model proposed by Roger and Moreau[12] is suitable for MAV rotor noise prediction. It is expected to be satisfactory for engineering purposes. Note that a high standard deviation is observed on the measurements at $4,500$ rpm. It might indicate the triggering of a vortex shedding phenomenon as a consequence of the leading seperation suspected from figure 3 as discussed in reference[16]. The possibility of an hysteresis effect is under investigation. Looking at the acoustic power spectrum $L_{wA}f$ can indicate the reason behind the overestimation of the two numerical tool. Acoustic power spectra are showed on figure 5 from the measurements and the numerical tools, namely, the optimization tool with the interaction noise model activated and the FWH–LBM aeroacoustic solver. On the one hand, the optimization tool overestimates the acoustic power as a result of the interaction noise model which yields a monotonically increasing spectrum resulting in high acoustic power at relatively high frequencies (beyond $2,000$ Hz). On the other hand, the FWH–LBM tool overestimates the energy radiated at the blade passing frequency (in the 315 Hz centered frequency band) and that drives the total acoustic power predicted.

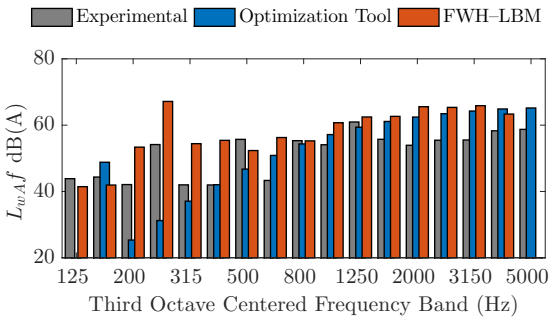

Figure 5: Acoustic power level at $5,000$ rpm from measurements and numerical predictions.

The acoustic predicted by the LBM simulation is studied based on predictions from the FWH–LBM tool and from direct measurements in the LBM simulation. That overestimation of the blade passing frequency is observed on the acoustic power spectral density (PSD) plotted in figure 6 both from the FWH–LBM tool and the direct measurements of the LBM simulation. The signals are taken in the rotor plane, corresponding with one microphone position, 1 m away from the rotor. Numerical predictions observed in figure 6 is a preliminary results: the PSD seems higher for every frequency than the measurements and that might be a consequence of the large frequency resolution available from the LBM simulations. The spectral densities are in general agreement and the FWH–LBM tool proves its relevance at higher frequencies. In this domain, mesh discretization of the LBM simulation reaches the same order of magnitude than the acoustic wavelength and a significant dissipation occurs.

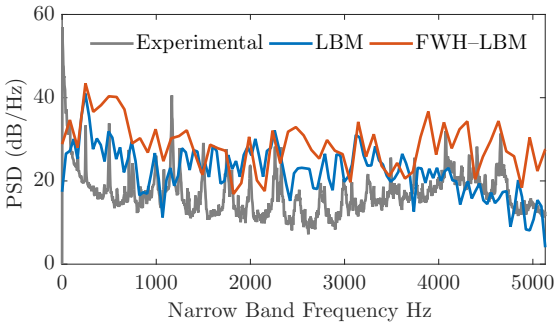

Figure 6: Acoustic power spectral density (PSD) from measurements and numerical predictions from LBM simulation at one microphone position in the rotor plane.

6 INTERACTING ON THE LEADING EDGE

From the previous investigation, the leading edge of the proposed optimized rotor is a key parameter to allow higher noise reduction: *i)* there is evidence of a leading edge separation that reduces the aerodynamic performances and

impinges the following blade and *ii)* turbulence interaction noise (or leading edge noise) is seen as the dominant source of noise. A passive device for flow control might then be a good option to enhance the aerodynamic performances and reduce the leading edge noise. One solution is a series of vortex generators to prevent flow separation[21]. Another solution, that currently receives a lot of attention, is leading edge turbercles, suggested by Fish and Battle and inspired by humpack whale flippers[22]. An early experimental investigation as been carried out by Soderman[23] yielding potential benefits. Investigation through LBM simulation is expensive, specially in an optimization context. A possible solution is the implementation in the optimization tool of a model that estimates the effect of leading edge waviness on acoustic radiation according to[24]. Three designs of wavy leading edge are presented and their respective chord distribution laws are plotted in figure 7.

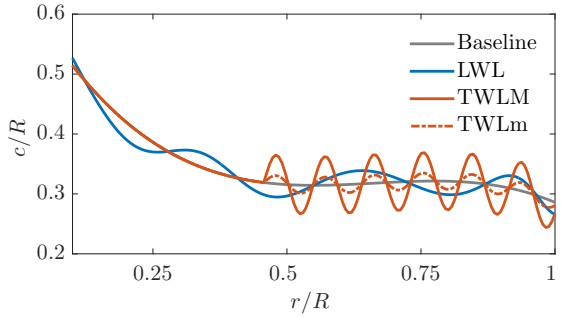

Figure 7: Chord distribution laws for the optimized rotor with straight and wavy leading edges.

Experimental and numerical investigation with LBM simulation has been carried out for one wavelength and one amplitude following the work of Favier *et al.*[25]. This is the first design referred to as "LWL" that stands for Large WaveLength. A more recent work published by Chaitanya *et al.*[26] suggests to scale the wavy leading edge wavelength with the turbulence length scale. However, there is no evidence to suggest that it holds for a rotary wing. Experimental investigation has been carried out for a optimized rotor with wavy leading edge wavelength based on the Taylor micro–scale retrieved from the LBM simulation. These are the second and third designs referred to as "TWLM" and "TWLm" that stands for Taylor WaveLength with high and low amplitude respectively. An experimental parametric study is under investigation by the authors to find the best geometrical properties of such serrations for rotors or propellers. No particular benefit on the acoustic reduction has yet been observed although a significant enhancement in aerodynamic performances is suspected for low wavelength and high amplitude serrations (such as the leading edge with serrations based on the Taylor micro–scale). The effect of the leading edge treatments on the aerodynamic performances are presented in table 1 for the thrust coefficient and the figure of merit at two rotational speeds. The thrust and torque coefficients and the figure of merit, respectively C_t, C_q and FM are defined as

$$C_t = \frac{T}{\frac{1}{2}\rho(\omega R)^2 \pi R^2} \; ; \; FM = \frac{T^{3/2}}{\omega Q \sqrt{2\rho\pi R^2}} \tag{1}$$

where T is the thrust, Q is the torque, ρ is the ambient density, ω is the rotational frequency and R is the rotor radius.

Table 1: Measurements of aerodynamic performances of the optimized rotor with straight and wavy leading edges.

		Baseline	LWL	TWLM	TWLm
3,000 rpm	C_t	0.08	0.08	0.09	0.08
	FM	0.71	0.65	0.50	0.73
5,000 rpm	C_t	0.08	0.08	0.10	0.08
	FM	0.69	0.76	0.57	0.82

The wavy leading edge with large wavelength ("LWL") has a predominant effect on torque. The thrust coefficient is almost unaffected for the two rotational speeds while the figure of merit decreases at lower rotational speeds and increases at higher rotational speed. The wavy leading with a wavelength based on the Taylor micro–scale and a high amplitude ("TWLM") has a high thrust coefficient at every rotational speeds but the figure of merit is lower which shows that the torque is very high for this configuration. Conversely, the wavy leading with a wavelength based on the Taylor micro–scale and a low amplitude ("TWLm") does not affect the thrust coefficient but significantly increases the figure of merit up to 20%, indicating that torque is reduced. The figure of merit for the optimized rotor with straight leading edge is decreasing with the rotational speed while it is increasing for every leading edge treatments. The effect of the leading edge treatments on the acoustic radiation is now presented in table 2 for the acoustic power at 5,000 rpm. The corresponding acoustic power spectra are plotted in figure 8.

Table 2: Acoustic power at 5,000 rpm from measurements for the optimized rotor with straight and wavy leading edges.

	Baseline	LWL	TWLM	TWLm
L_{wA} dB(A)	69.9	69.3	72.2	68.83

The acoustic power is systematically reduced with the use of leading edge treatments except when the wavelength is based on the Taylor micro–scale with a high amplitude ("TWLM"). The most important noise reduction is achieved when the wavelength is based on the Taylor micro–scale with a low amplitude ("TWLm") and that correspond to the case of higher figure of merit. That indicates that the optimization tool combined with a suitable leading edge treatment of low wavelength and low amplitude can enhance the aerodynamic performance and reduce acoustic radiation.

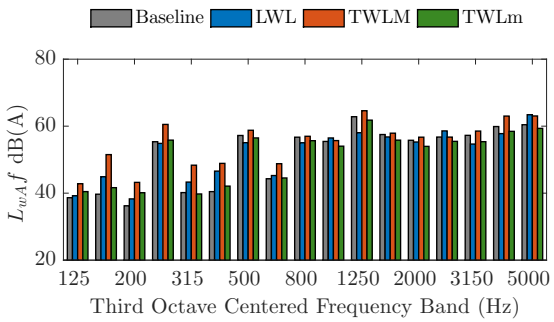

Figure 8: Acoustic power level at $5,000$ rpm from measurements for the optimized rotor with straight and wavy leading edges.

The corresponding acoustic power spectra showed in figure 8 bring insight on the noise reduction mechanisms. The low frequencies are higher for every leading edge treatments while the high frequencies are lower: *i)* the acoustic energy is more equally distributed over the frequency range and *ii)* as acoustic energy is shifted from the high frequencies to the low frequencies, less radiated energy is perceived by the observer as a result of A–weighting filtering. Two mechanisms to explain noise reduction by leading edge tubercles can be found in references [26] and [27]. Wang *et al.* [27] indicates that leading edge tubercles are efficient to prevent leading edge separation and that in turns reduces vortex shedding noise that is fed by that flow separation and shed in the wake. Clair *et al.* [28] suggest that it is efficient to reduction turbulence interaction noise and the explanation is provided by [26] in the form of a sound wave cancellation phenomenon where acoustic sources are forced to be localized in the through.

7 CONCLUSIONS

An optimization tool is developped for engineering purposes and has proven its effectiveness to reduce noise produced by MAV rotors in hover and increase endurance. An experimental protocol is designed for non–treated rooms. Comparisons with measurements in anechoic environments are to follow. In MAV rotors, the dominant source of noise is found to be produced by the interaction between turbulence and leading edge. Higher level of noise reduction are expected in the future using appropriate leading edge treatments.

ACKNOWLEDGEMENTS

This research is supported by the Direction Générale de l'Armement (DGA) from the French Ministry of Defense. The authors thank the technical team for their support and specially Rémy Chanton from for the set–up of the aerodynamic balance and Sylvain Belliot for the rapid prototyping.

References

[1] A. Pagano, M. Barbarino, D. Casalino, and L. Federico. Tonal and broadband noise calculations for aeroacoustic optimization of propeller blades in a pusher configuration. In *15th AIAA/CEAS Aeroacoustics Conference*, number AIAA-2009-3138, 2009.

[2] S. Pednekar, D. Ramaswamy, and R. Mohan. Helicopter rotor noise optimization. In *5th Asian-Australian Rotorcraft Forum*, 2016.

[3] C. F. Wisniewski, A. R. Byerley, W. H. Heiser, K. W. Van Treuren, and W. R. Liller. Designing small propellers for optimum efficiency and low noise footprint. In *33rd AIAA Applied Aerodynamics Conference*, number AIAA-2015-2267, 2015.

[4] N. S. Zawodny, D. Douglas Boyd Jr, and C. L. Burley. Acoustic characterization and prediction of representative, small–scale rotary–wing unmanned aircraft system components. In *72nd AHS Annual Forum*, 2016.

[5] R. Serré, V. Chapin, J. M. Moschetta, and H. Fournier. Reducing the noise of micro–air vehicles in hover. In *International Micro Aerial Vehicle Conference*, 2017.

[6] H. Winarto. BEMT algorithm for the prediction of the performance of arbitrary propellers. Melbourne: The Sir lawrence Wackett Centre for Aerospace Design Technology, Royal Melbourne Institute of Technology, 2004.

[7] C. A. Lyon, A. P. Broeren, P. Giguère, A. Gopalarathnam, and M. S. Selig. Summary of low–speed airfoil data volume 3. SoarTech Publications, Virginia Beach, VA, 1998.

[8] J. Morgado, R. Vizinho, M. A. R. Silvestre, and J. C. Páscoa. XFOIL *vs* CFD performance predictions for high light low Reynolds number airfoils. *Aerospace Science and Technology*, 52:207–214, 2016.

[9] M. Drela and M. B. Giles. Viscous–inviscid analysis of transonic and low Reynolds number airfoils. *AIAA Journal*, 25(10):1347–1355, 1987.

[10] G. Sinibaldi and L. Marino. Experimental analysis on the noise of propellers for small UAV. *Applied Acoustics*, 74:79–88, 2013.

[11] J. E. Ffowcs Williams and D. L. Hawkings. Sound generation by turbulence and surfaces in arbitrary motion. *Philosophical Transactions of the Royal Society of London*, 264(1151):321–342, 1969.

[12] M. Roger and S. Moreau. Extensions and limitations of analytical airfoil broadband noise models. *International Journal of Aeroacoustics*, 9(3):273–305, 2010.

[13] D. Casalino. An advanced time approach for acoustic analogy predictions. *Journal of Sound and Vibration*, 261:583–612, 2003.

[14] F. Farassat and G. P. Succi. A review of propeller discrete frequency noise prediction technology with emphasis on two current methods for time domain calculations. *Journal of Sound and Vibration*, 71(3):399–419, 1980.

[15] Y. N. Kim and A. R. George. Trailing–edge noise from hovering rotors. *AIAA Journal*, 20(9):1167–1174, 1982.

[16] R. Serré, N. Gourdain, T. Jardin, A. Sabaté López, V. Sujjur Balaramraja, S. Belliot, M. C. Jacob, and J. M. Moschetta. Aerodynamic and acoustic analysis of an optimized low reynolds number rotor. In *17th International Symposium on Transport Phenomena and Dynamics of Rotating Machinery*, 2017.

[17] X. Gloerfelt, C. Bailly, and D. Juvé. Direct computation of the noise radiated by a subsonic cavity flow and application of integral methods. *Journal of Sound and Vibration*, 266:119–146, 2003.

[18] G. A. Brès, F. Pérot, and D. Freed. A Ffowcs Williams–Hawking solver for Lattice–Boltzmann based computation aeroacoustics. In *16th AIAA/CEAS Aeroacoustics Conference*, number AIAA-2010-3711, 2010.

[19] L. V. Lopes, D. Douglas Boyd Jr, D. M. Nark, and K. E. Wiedemann. Identification of spurious signals from permeable Ffowcs Williams and Hawkings surfaces. In *73nd AHS Annual Forum*, 2017.

[20] D. P. Lockard. An efficient, two–dimensional implementation of the Ffowcs Williams and Hawkings equation. *Journal of Sound and Vibration*, 229(4):897–911, 2000.

[21] J. C. Lin. Review of research on low–profile vortex generators to control boundary-layer separation. *Progress in Aerospace Sciences*, 38:389–420, 2002.

[22] F. E. Fish and J. M. Battle. Hydrodynamic design of the Humpback Whale flipper. *Journal of morphology*, 225:51–60, 1995.

[23] P. T. Soderman. Leading-edge serrations which reduce the noise of low-speed rotors. NASA, Technical note no. D-7371, 1973.

[24] B. Lyu, M. Azarpeyvand, and S. Sinayoko. Noise prediction for serrated leading–edges. In *22nd AIAA/CEAS Aeroacoustics Conference*, number AIAA-2016-2740, 2016.

[25] J. Favier, A. Pinelli, and U. Piomelli. Control of the separated flow around an airfoil using a wavy leading edge inspired by humpback whale flippers. *C. R. Mecanique*, 340:107–114, 2012.

[26] P. Chaitanya, P. Joseph, S. Narayanan, C. Vanderwel, J. Turner, J. W. Kim, and B. Ganapathisubramani. Performance and mechanism of sinusoidal leading edge serrations for the reduction of turbulence–aerofoil interaction noise. *Journal of Fluid Mechanics*, 818:435–464, 2017.

[27] J. Wang, C. Zhang, Z. Wu, J. Wharton, and L. Ren. Numerical study on reduction of aerodynamic noise around an airfoil with biomimetic structures. *Journal of Sound and Vibration*, 394:46–58, 2017.

[28] V. Clair, C. Polacsek, T. Le Garrec, G. Reboul, M. Gruber, and P. Joseph. Experimental and numerical investigation of turbulence–airfoil noise reduction using wavy edges. *AIAA Journal*, 51(11):2695–2713, 2013.